

The onset of nanoscale dissipation in superfluid ^4He at zero temperature: The role of vortex shedding and cavitation

Francesco Ancilotto¹, Manuel Barranco², Martí Pi², and Jussi Eloranta³

¹*Dipartimento di Fisica e Astronomia “Galileo Galilei” and CNISM,
Università di Padova, via Marzolo 8, 35122 Padova,*

Italy and CNR-IOM Democritos, via Bonomea, 265 - 34136 Trieste, Italy

²*Departament FQA, Facultat de Física, Universitat de Barcelona. Diagonal 645, 08028 Barcelona,
Spain and Institute of Nanoscience and Nanotechnology (IN2UB), Universitat de Barcelona.*

³*Department of Chemistry and Biochemistry, California State University at Northridge, California 91330, USA*

(Dated: June 29, 2021)

Two-dimensional flow past an infinitely long cylinder of nanoscopic radius in superfluid ^4He at zero temperature is studied by time-dependent density functional theory. The calculations reveal two distinct critical phenomena for the onset of dissipation: 1) vortex-antivortex pair shedding from the periphery of the moving cylinder and 2) appearance of cavitation in the wake, which possesses similar geometry as observed experimentally for fast moving micrometer-scale particles in superfluid ^4He . Vortex pairs with the same circulation are occasionally emitted in the form of dimers, which constitute the building blocks for the Benard-von Karman vortex street structure observed in classical turbulent fluids and Bose-Einstein condensates (BEC). The cavitation induced dissipation mechanism should be common to all superfluids that are self-bound and have a finite surface tension, which include the recently discovered self-bound droplets in ultracold Bose gases.

PACS numbers: 67.25.dg, 67.25.dk, 67.85.-d

One of the manifestations of ^4He superfluidity at zero temperature (T) is the frictionless liquid flow through capillaries at sufficiently low velocities. Based on the well-known Landau criterion, the onset of dissipation is related to the unusual form of the superfluid dispersion relation, $\epsilon(p)$, which exhibits roton minimum $\epsilon(p_{min})$ at p_{min} . The flow should become dissipative when the velocity reaches the critical Landau value $v_L = \epsilon(p_{min})/p_{min} = 59$ m/s [1]. Similarly, an object moving in superfluid ^4He should experience drag only above a certain critical velocity threshold v_c . It is well established experimentally that objects moving already at much lower velocities than v_L experience drag due to the emission of non-linear excitations in the form of quantized vortices; see for example Ref. [1].

Multiple interacting vortices in a superfluid can form a well-defined lattice or a more complicated vortex tangle, depending on their geometry and circulation. At high vortex densities, vortex reconnection events, which are believed to be responsible for the large-scale behavior of quantum turbulence [2–5], become increasingly important. Quantum turbulence is associated with the proliferation of quantized vortices [6, 7]. From the experimental point of view, vorticity can be created by stirring or rotating the superfluid [8–10].

Although quantized vorticity plays a key role in the onset of dissipation in superfluid flows, a fundamental understanding of their role in exerting drag on moving objects and the dependence of the associated critical velocity on the object size is still lacking. In this paper, we identify a new, previously overlooked, energy dissipation mechanism that takes place also well below v_L . The energy loss and the induced drag force on the object

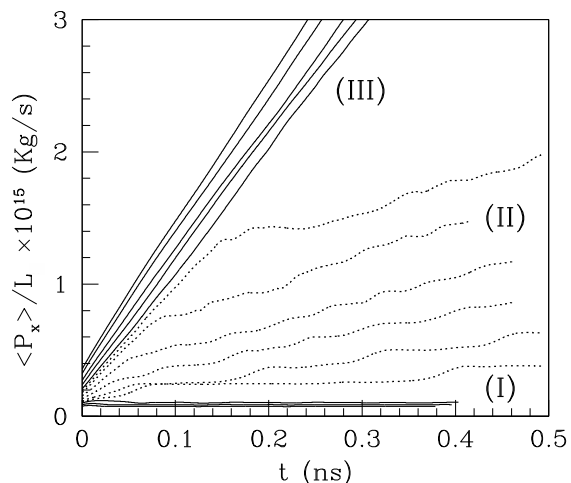


FIG. 1: Linear momentum per unit length around a cylinder with radius $R = 3$ Å as a function of time. The curves shown refer to different values of the cylinder velocity. In group (I) they correspond to $v = 0.44, 0.48,$ and 0.52 (in units of v_L). In group (II), from bottom to top they correspond to $v = 0.55, 0.57, 0.61, 0.66, 0.70,$ and 0.72 . In group (III), the velocities are from bottom to top $v = 0.74, 0.79, 0.83, 0.89,$ and 0.94 .

in this mechanism originate from the formation of cavitation bubbles in the wake. Cavitation bubbles play a crucial role in the appearance of drag as they may act as vortex nucleation seeds through local distortions of their surface and, more importantly, their nucleation and growth provides a significant source of energy loss.

We have studied the onset of dissipation in superfluid ^4He at $T = 0$ by simulating two-dimensional flow past an

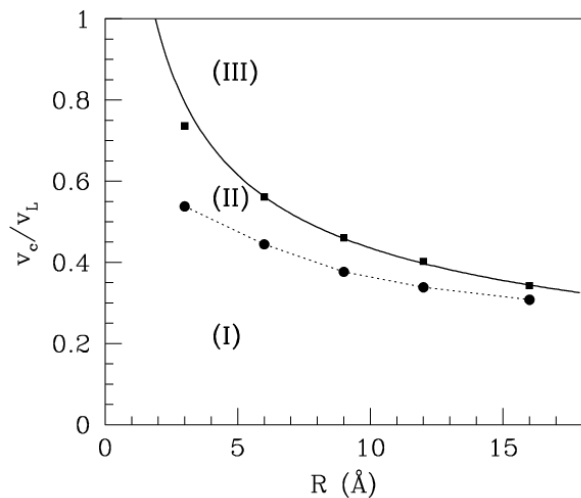


FIG. 2: Critical velocities v_{c1} (filled circles) and v_{c2} (filled squares) as a function of the cylinder radius. The solid line shows a fit of $R^{-1/2}$ law to v_{c2} whereas the dotted line is just provided as a guide to the eye. The Roman numbers refer to the three different regions identified in Fig. 1.

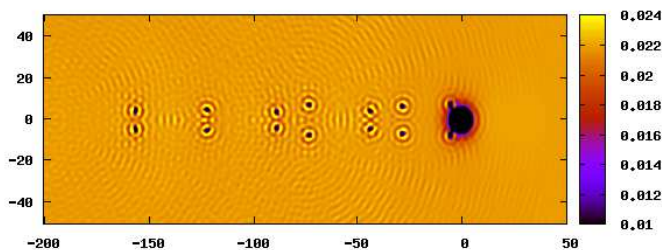


FIG. 3: A snapshot of liquid helium density around a moving cylinder ($R = 3 \text{ \AA}$) at constant velocity $v = 0.66 v_L$ (regime II). The cylinder, located at the origin in the xy -plane, is about to emit a vortex pair. The lengths are expressed in \AA and density contours in \AA^{-3} .

infinitely long cylinder (wire) with a nanoscopic cross-section using time-dependent density functional theory (TDDFT). The employed 2D wire geometry is not only simpler to simulate than the full three-dimensional case associated with, e.g., a moving sphere, but it is also appealing because vibrating wire resonators are commonly used to study quantum turbulence in superfluid ^4He [11, 12].

The cylinder is represented in the calculations by a repulsive external potential, $V(r) = V_0[1 + e^{(r-R)/\sigma}]^{-1}$ with $r = \sqrt{x^2 + y^2}$, $\sigma = 0.3 \text{ \AA}$, and $V_0 = 5000 \text{ K}$. This potential represents a hard cylindrical object with radius R aligned along the z -axis. In the following, the liquid flow (or the cylinder motion) is oriented along the x -axis with a given velocity v .

Within DFT, superfluid ^4He is described by a complex valued order parameter (effective wave function)

$\Psi(\mathbf{r}, t)$, which is related to the atomic density as $\rho(\mathbf{r}, t) = |\Psi(\mathbf{r}, t)|^2$. In the cylinder frame of reference, the TDDFT equation becomes

$$i\hbar \frac{\partial}{\partial t} \Psi(\mathbf{r}, t) = \left\{ -\frac{\hbar^2}{2m} \nabla^2 + \frac{\delta \mathcal{E}_c}{\delta \rho} + V(r) - v \hat{P}_x \right\} \Psi(\mathbf{r}, t) \quad (1)$$

where $\hat{P}_x = -i\hbar \partial / \partial x$ is the linear momentum operator along the x -axis and the functional $\mathcal{E}_c[\rho]$ was taken from Ref. [13]. This functional includes both finite-range and non-local corrections that are required to describe the $T = 0$ response of liquid ^4He on the Ångström-scale accurately. Due to the translational invariance, the problem reduces to finding the fluid density and velocity field in the (x, y) -plane. The details on solving the TDDFT equation can be found from Ref. [14]. Previously, DFT models with various levels of complexity have been used to study the motion of electrons and ions in liquid ^4He as well as the mechanism of vortex ring emission; see, e.g., Refs. [15–17] and references therein.

Equation (1) was solved for wire radii $R = 3, 6, 9, 12$, and 16 \AA at several fixed values of velocity. The force per unit length exerted on the superfluid by the moving object can be calculated from the momentum transfer rate to the fluid

$$F_d = \frac{1}{L} \frac{\partial \langle \hat{P}_x \rangle}{\partial t} = \frac{1}{L} \frac{\partial}{\partial t} \left[\int d\mathbf{r} \Psi^*(\mathbf{r}, t) \hat{P}_x \Psi(\mathbf{r}, t) \right] \quad (2)$$

where L is the length of the wire. The onset of drag was identified by observing the time dependence of $\langle \hat{P}_x \rangle / L$.

Figure 1 shows the time dependence of $\langle \hat{P}_x \rangle / L$ for $R = 3 \text{ \AA}$ at selected values of flow velocity. According to Eq. (2), the drag force acting on the moving object corresponds to the slope of the curves shown. At variance with previously reported results for objects moving in superfluid BECs, where a single critical velocity separates inviscid flow from the onset of drag due to vortex shedding [8, 18], we find *two distinct critical velocities* for superfluid ^4He . These velocities, which in the following are denoted by v_{c1} and v_{c2} , separate three different regimes: (I) inviscid flow, (II) vortex pair shedding, and (III) cavitation bubble formation.

For object velocities $v < v_{c1}$ (regime I), the fluid profile around the object converges rapidly with time into a stationary configuration. Both the density and the velocity field for such configurations are fore-to-aft symmetric. This implies that the drag force on the object is zero (flat portion of the curves (I) in Fig. 1), which is the well-known D’Alembert paradox for classical fluids. Fig. 1 also shows that in the other two regimes, the time-dependent behavior of the total momentum is characterized by notable transient periods where the wire experiences a higher drag due to the tendency of developing a cavity around the object. Furthermore, depending on the wire velocity, the slope may then either decrease and settle to a lower value (regime II), or remain approximately constant (regime III).

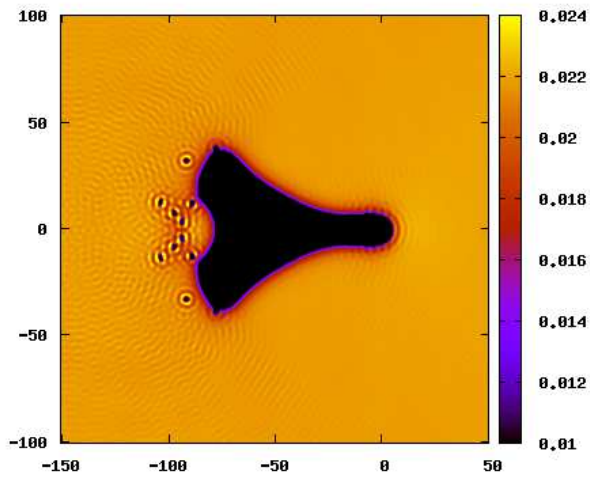


FIG. 4: A snapshot of the liquid density around a cylinder ($R = 3 \text{ \AA}$) moving at $v = 0.79 v_L$ (regime III). The cylinder is located at the origin in the xy -plane. The lengths are expressed in \AA and density contours in \AA^{-3} .

When the velocity exceeds v_{c1} , singly-quantized linear vortex-antivortex pairs are nucleated periodically on both sides of the wire cross-section. The vortices eventually detach from the object and drift downstream as vortex dipoles. Their appearance is accompanied by drag force acting on the moving wire, which increases with velocity (group of curves labeled (II) in Fig. 1). The oscillations in the dotted curves after the initial period reflect the quasi-periodic emission of vortex pairs. In this regime, the cavity around the object largely recovers its circular geometry after each vortex emission event. As the velocity is increased, the vortex shedding frequency is observed to increase accordingly. Overall, this behavior is similar to BECs where quasi-periodic vortex-antivortex pair emission events also take place [19–21].

Finally, in regime (III) ($v > v_{c2}$), the response of the fluid environment close to the moving wire changes dramatically as empty cavities are formed in the wake. This cavity formation is accompanied by simultaneous quasi-periodic emission of vortex pairs. Note that the transition between regimes (II) and (III) is characterized by a discontinuous jump in the drag force exerted on the cylinder due to the formation of bubbles (see Fig. 1).

Cavitation is initiated by an asymmetric fore-to-aft density profile such that the liquid density decreases substantially behind the moving wire, thus resulting in a reduction of the local pressure. If the velocity is sufficiently high, this density decrease can trigger the formation of bubbles around or behind the wire. A similar mechanism is also responsible for cavitation in liquid ^4He at negative pressures [22, 23].

The critical velocities v_{c1} and v_{c2} , where the transitions to the dissipative regimes (II) and (III) take place, are

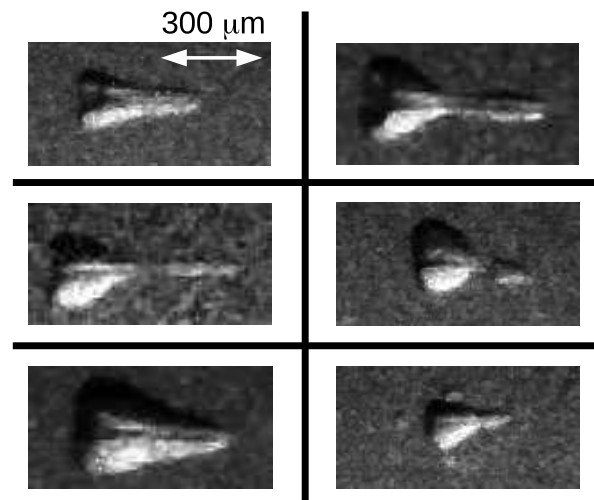


FIG. 5: An overview of the bubble shapes observed around fast moving metal particles (diameter few microns) propagating from left to right in superfluid ^4He at 1.7 K (saturated vapor pressure). The data shown correspond to the observations made during the experiments described in Ref. [25].

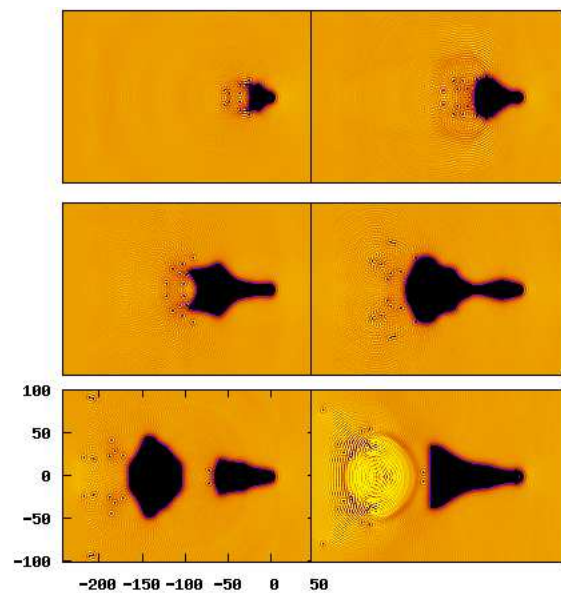


FIG. 6: Time evolution of the liquid density around a moving cylinder ($R = 3 \text{ \AA}$) at constant velocity $v = 0.74 v_L$ (regime III). The snapshots are taken between $t = 0.15 \text{ ns}$ (top left panel) and $t = 0.65 \text{ ns}$ (bottom right panel). The lengths are expressed in \AA and density contours in \AA^{-3} according to the scale specified in Fig. 4.

shown in Fig. 2 as a function of R . At the nanoscale, the velocities exhibit distinct dependencies on the cylinder radius, but for large radii v_{c1} and v_{c2} seem to converge towards a single value. Therefore, at the mesoscale, the onset of vortex shedding and bubble cavitation should appear simultaneously at a common critical velocity value

v_c . Furthermore, v_c decreases with increasing R , which is in accordance with the existing experimental data showing that the actual critical velocities are lower than v_L (e.g., cm/s or even mm/s values are usually measured) [1, 12].

Figure 3 shows a snapshot taken during real-time evolution of the system with $R = 3 \text{ \AA}$ and $v = 0.3 v_L > v_{c1}$ (regime II) [24]. Singly quantized vortex pairs with opposite circulation (vortex dipoles) are emitted behind the moving wire. Note that for a spherical object in 3D, the emitted vortex dipoles would be vortex rings instead [15–17]. The overall vortex emission process is quasi-periodic, and the frequency of vortex shedding events increases with velocity v , which is consistent with experimental observations in superfluid ^4He [21].

For a cylinder with $R = 3 \text{ \AA}$, Fig. 4 shows a transient image corresponding to $v = 0.79 v_L > v_{c2}$ (regime III). In addition to vortex dipole emission, formation of a wide dynamically evolving cavity is observed. Remarkably, in spite of the fact that the shapes and volumes of such cavities continuously change in time, their hydrodynamic drag remains approximately constant. This is evidenced by the fact that the slopes of the solid lines in Fig. 1 (regime III) do not vary significantly as a function of time.

Very similar cavity shapes that appear in regime III have been observed in recent experiments where micrometer-scale metal particles were injected into bulk superfluid helium by laser ablation [25]. The main features of the observed fast propagating particle-bubble systems were the elongated cavity geometry and the widened flat or cone-shaped tail structure (see Fig. 5), which are both clearly reproduced by the present simulations. Note that an exact match between the cavity geometries in the experiments and the present simulations is not expected due to the different object geometries (i.e., sphere vs. cylinder), the presence of gaseous insulating layer between the particle and the liquid (i.e., insulating Leidenfrost layer [26]), and the difference in length scales (nm vs. μm). Regarding the latter point, Fig. 2 shows that both vortex emission and cavitation processes in these experiments should take place at the same value of v_c .

In addition to the velocity dependent cavity shapes formed around the particles, a trail of slowly drifting cavitation bubbles were also observed behind the fast particles propagating in the liquid [25]. This is a direct consequence of particle-cavitation bubble splitting, which is reproduced by the present simulations as demonstrated in Fig. 6. When the bubble detaches, the leading portion hosts the object and the trailing bubble is left empty. As shown by the two bottom panels of Fig. 6, the trailing bubble eventually collapses and leads to the emission of shock waves.

The moving object may also emit closely spaced vortex dimers in the wake, i.e., bound pairs of vortices with the

same direction of circulation, which are different from the vortex dipoles discussed above. Once formed, each dimer structure remains bound and rotates around its center of mass while moving away from the cavity that hosts the wire.

The formation of vortex dimers behind the object is the hallmark of well-known phenomenon in classical fluid dynamics at large Reynolds numbers, i.e. the Benard-Von Karman (BvK) vortex street, where an incompressible flow past an object produces an asymmetric wake downstream consisting of quasi-periodically nucleated vortex dimers. Such BvK vortex street structures have been observed experimentally in BECs and simulated by the time-dependent Gross-Pitaevskii (GP) equation [8, 27], but so far were never observed in superfluid helium.

The upper critical velocity for cavitation, v_{c2} , appears to follow the $v_c \propto R^{-1/2}$ law as indicated by the solid line in Fig. 2. This behavior is similar to the onset of drag when liquid ^4He is forced to flow through a cylindrical channel of diameter d where the critical velocity was found to scale as $v_c \sim d^{-1/2}$ [28]. In BECs, the experiments of Kwon *et al.* [18], where vortex shedding was produced by a laser beam of “radius” R moving through the condensate, show a $1/R^s$ dependence of the critical velocity with $s < 1$.

Several studies have, however, suggested a scaling law $v_c \propto 1/R$. For example, the superfluid Reynolds number Re_s was introduced [29–31] by replacing the kinematic viscosity ν with quantized circulation $\kappa = h/m$ in the definition of Reynolds number, $\text{Re} = Dv/\nu$, yielding $\text{Re}_s \sim mvD/h$ where D is the characteristic size of the system. This model has been employed to analyze oscillating sphere data in superfluid ^4He in the mK regime [29–31] where a critical Re_s value for the appearance of turbulent behavior was determined. Similar conclusions were also drawn from simulations for the onset of turbulent flow in BECs [29, 32]. The existence of a threshold value for Re_s implies that the associated critical velocity v_c must scale as $1/R$, which is different from our result for superfluid helium. At present, the situation regarding the scaling law thus remains inconclusive.

In summary, we have shown that the formation of cavitation bubbles plays an important role in the onset of dissipation in superfluid ^4He , which is at variance with the accepted view that only vorticity should be responsible for such behavior. It is worth noticing that the reported cavitation dissipation mechanism is not applicable to cold gas BECs because they are not self-bound and have no surface tension. However, the recently observed self-bound droplets in ultracold dipolar bosonic gas [33] could provide an interesting test ground for exploring this mechanism further.

We thank Antonio Muñoz and Leticia Tarruell for useful discussions. This work was performed under Grants No 2014SGR401 from Generalitat de Catalunya, FIS2014-52285-C2-1-P from DGI (Spain) and DMR-

1205734 from NSF (USA).

-
- [1] J. Wilks, *The properties of liquid and solid Helium*, International Series of Monographs on Physics (Clarendon, Oxford, 1967).
- [2] R.M. Kerr, Phys. Rev. Lett. **106** 224501 (2011).
- [3] R. Tebbs, A.J. Youd, and C. Barenghi, J. Low Temp. Phys. **162**, 314 (2011).
- [4] S. Ogawa, M. Tsubota, and Y. Hattori, J. Phys. Soc. Japan **71**, 813 (2002).
- [5] J. Koplik and H. Levine, Phys. Rev. Lett. **71**, 1375 (1993);
- [6] W.F. Vinen, J. Low Temp. Phys. **145**, 7 (2006).
- [7] M.S. Paoletti and D.P. Lathrop, Annu. Rev. Condens. Matter Phys. **2**, 213 (2011).
- [8] W.J. Kwon, J.H. Kim, S.W. Seo, and Y. Shin, Phys. Rev. Lett. **117**, 245301 (2016).
- [9] J.R. Abo-Shaeer, C. Raman, J.M. Vogels, and W. Ketterle, Science **292**, 476 (2001).
- [10] S. Inouye, S. Gupta, T. Rosenband, A. P. Chikkatur, A. Gorlitz, T.L. Gustavson, A. E. Leanhardt, D. E. Pritchard, and W. Ketterle, Phys. Rev. Lett. **87**, 080402 (2001).
- [11] R.Goto, S. Fujiyama, H. Yano, Y. Nago, N. Hashimoto, K. Obara, O. Ishikawa, M. Tsubota, and T. Hata, Phys. Rev. Lett. **100**, 045301 (2008).
- [12] D.I. Bradley *et al.*, J. Low Temp. Phys. **154**, 97 (2009).
- [13] F. Ancilotto, M. Barranco, F. Caupin, R. Mayol, and M. Pi, Phys. Rev. B **72**, 214522 (2005).
- [14] D. Mateo, D. Jin, M. Pi, and M. Barranco, J. Chem. Phys. **134**, 044507 (2011).
- [15] N.G. Berloff and P.H. Roberts, Phys. Lett. A **274**, 69 (2000).
- [16] D. Jin and W. Guo, Phys. Rev. B **82**, 094524 (2010).
- [17] F. Ancilotto, M. Barranco, and M. Pi, Phys. Rev. B **82** 014517 (2010).
- [18] W.J. Kwon, G. Moon, S.W. Seo, and Y. Shin, Phys. Rev. A **91**, 053615 (2015).
- [19] T. Frisch, Y. Pomeau, and S. Rica, Phys. Rev. Lett. **69**, 1644 (1992).
- [20] T. Winiecki, B. Jackson, J.F. McCann, and C.S. Adams, J. Phys. B: At. Mol. Opt. Phys. **33**, 4069 (2000).
- [21] M. Niemetz, R. Hanninen and W. Schoepe, J. Low Temp. Phys. **187**, 195 (2017).
- [22] Q. Xiong and H.J. Maris, J. Low Temp. Phys. **77**, 347 (1989).
- [23] S. Balibar, J. Low Temp. Phys. **129**, 363 (2002).
- [24] The Landau critical velocity for the applied functional (see Ref. [13]) is $v_L = 94.4$ m/s, which is larger than the experimental value (59 m/s). Despite this difference, our simulations show that neither vortex nor bubble nucleation are connected to the presence of roton minimum or the associated Landau velocity. To facilitate comparison with experiments, we present the results relative to v_L of the functional.
- [25] X. Buelna, A. Freund, D. Gonzalez, E. Popov, and J. Eloranta, J. Phys. Chem. B **120**, 11010 (2016).
- [26] I.U. Vakarelski, J.O. Marston, D.Y.C. Chan, and S.T. Thoroddsen, Phys. Rev. Lett. **106** 214501 (2011).
- [27] G.W. Stagg, N.G. Parker, and C.F. Barenghi, J. Phys. B: At. Mol. Opt. Phys. **47**, 095304 (2014).
- [28] A.C. Biswas and R.K. Pathria, J. Low Temp. Phys. **28**, 151 (1977).
- [29] M.T. Reeves, T.P. Billam, B.P. Anderson, and A.S. Bradley, Phys. Rev. Lett. **114**, 155302 (2015).
- [30] A.P. Finne, T. Araki, R. Blaauwgers, V.B. Eltsov, N.B. Kopnin, M. Krusius, L. Skrbek, M. Tsubota, and G.E. Volovik, Nature **424**, 1022 (2003).
- [31] W. Schoepe, JETP Letters **102**, 105 (2015).
- [32] J.S. Stieberger and W. Zwerger, Phys. Rev. A **62**, 061601(R) (2000).
- [33] M. Schmitt, M. Wenzel, F. Böttcher, I. Ferrier-Barbut, and T. Pfau, Nature **539**, 259 (2016).